

Elastocaloric and multicaloric effects in magnetoelastic coupled Ni-Mn-based Heusler shape memory alloys

Yuetong Sun(孙悦彤) and Jian Liu(刘剑)
Citation: Chin. Phys. B, 2026, 35 (**7**): 078103. DOI: 10.1088/1674-1056/ae3607
http://cpb.iphy.ac.cn; http://iopscience.iop.org/cpb

What follows is a list of articles you may be interested in

Pre-existing orthorhombic embryos-induced hexagonal—orthorhombic martensitic transformation in $MnNiSi_{1-x}(CoNiGe)_x$ alloy

Ting-Ting Zhang(张婷婷), Yuan-Yuan Gong(龚元元), Zi-Qian Lu(鲁子骞), and Feng Xu(徐锋)
Chin. Phys. B, 2024, 33 (**4**): 048103. DOI: 10.1088/1674-1056/ad188d

High temperature strain glass in Ti-Au and Ti-Pt based shape memory alloys

Shuai Ren(任帅), Chang Liu(刘畅), and Wei-Hua Wang(汪卫华)
Chin. Phys. B, 2021, 30 (**1**): 018101. DOI: 10.1088/1674-1056/abc54a

Evolution of magnetic domain structure of martensite in Ni-Mn-Ga films under the interplay of the temperature and magnetic field

Xie Ren (谢忍), Wei Jun (韦俊), Liu Zhong-Wu (刘仲武), Tang Yan-Mei (唐妍梅), Tang Tao (唐涛), Tang Shao-Long (唐少龙), Du You-Wei (都有为)
Chin. Phys. B, 2014, 23 (**6**): 068103. DOI: 10.1088/1674-1056/23/6/068103

Relation between martensitic transformation temperature range and lattice distortion ratio of NiMnGaCoCu Heusler alloys

Wei Jun (韦俊), Xie Ren (谢忍), Chen Le-Yi (陈乐易), Tang Yan-Mei (唐研梅), Xu Lian-Qiang (许连强), Tang Shao-Long (唐少龙), Du You-Wei (都有为)
Chin. Phys. B, 2014, 23 (**4**): 048107. DOI: 10.1088/1674-1056/23/4/048107

Thermal stability and high-temperature shape memory characteristics of Ti-20Zr-10Ta alloy

Zheng Xiao-Hang (郑晓航), Sui Jie-He (隋解和), Zhang Xin (张欣), Yang Zhe-Yi (杨哲一), Cai Wei (蔡伟)
Chin. Phys. B, 2014, 23 (**1**): 018101. DOI: 10.1088/1674-1056/23/1/018101

TOPICAL REVIEW — Multiferroicity and multicaloric effects

Elastocaloric and multicaloric effects in magnetoelastic coupled Ni–Mn-based Heusler shape memory alloys

Yuetong Sun(孙悦彤)[1,2] and Jian Liu(刘剑)[1,2,†]

[1] *State Key Laboratory of Materials for Advanced Nuclear Energy, Shanghai University, Shanghai* 200444, *China*
[2] *Institute of Material Research, School of Materials Science and Engineering, Shanghai University, Shanghai* 200444, *China*

(Received 10 November 2025; revised manuscript received 8 January 2026; accepted manuscript online 9 January 2026)

Ni–Mn-based Heusler shape memory alloys (SMAs), considered promising candidates for solid-state refrigeration, possess outstanding elastocaloric effect (eCE) and magnetocaloric effect (MCE) associated with their martensitic transformations (MTs). Driven by stress-induced MTs, the eCE involves the absorption and release of latent heat during the reversible phase transition. Additionally, a strong magnetic response emerges near the MT temperature, giving rise to a multicaloric effect. In this study, the mechanism of magnetoelastic coupling, relevant processing techniques, and multicaloric effects in Ni–Mn-based SMAs are reviewed.

Keywords: Ni–Mn-based alloys, elastocaloric effect, magnetocaloric effect, martensitic transformation

PACS: 81.30.Kf, 75.30.Sg, 62.20.fg, 46.25.Hf

DOI: 10.1088/1674-1056/ae3607 **CSTR:** 32038.14.CPB.ae3607

1. Introduction

With the escalating global energy crisis and greenhouse effect, the development of efficient and environmentally friendly refrigeration technologies has become a major research focus in energy materials. Traditional vapor-compression refrigeration technologies suffer from low energy efficiency and cause environmental pollution due to their reliance on greenhouse gas refrigerants.[1,2] Therefore, emerging refrigeration technologies based on solid-state phase transitions, such as elastocaloric, magnetocaloric, and multicaloric refrigeration, are regarded as promising approaches for next-generation green cooling.[3–5] Among the various solid-state refrigeration materials, Ni–Mn-based Heusler alloys have recently become prominent in functional material research. Their phase transitions can be triggered by both magnetic and mechanical fields, and the transition temperature can be precisely tuned by external stimuli, demonstrating substantial potential for elastocaloric and multicaloric applications.[6]

Ni–Mn–X (X = Ga, In, Sn, Sb, Ti) alloys can absorb or release large amounts of latent heat during the martensitic transformation (MT), producing significant adiabatic temperature changes under external stress or magnetic fields. Compared with other shape memory alloys, Ni–Mn-based alloys offer numerous advantages, including low phase-transition stress, small hysteresis, and tunable transition temperatures, making them particularly suitable for solid-state refrigeration and energy-conversion devices near room temperature (RT). However, their intrinsic brittleness limits their practical applications, including achieving long-term functional fatigue resistance over millions of cycles and broadening the operating temperature window to meet diverse cooling demands.[7–9] To overcome this drawback, researchers have explored two major strategies to improve their comprehensive performance: implementing advanced processing techniques and investigating off-stoichiometric compositions. Unlike traditional metallurgical methods, advanced technologies, such as directional solidification, additive manufacturing (AM), and magnetic-field-controlled solidification, promote the development of microstructures with low defect densities and strong textures. On the other hand, multi-element alloying enables precise control over the phase-transition temperature, hysteresis, and mechanical properties.

In this review, we systematically summarize recent progress on the elastocaloric effect (eCE) and multicaloric effects in Ni–Mn-based alloys, with emphasis on the influence of different preparation processes on microstructure and functional properties. We also discuss the role of main-group elements, transition metals, and rare-earth elements in optimizing phase-transition behavior and mechanical properties, and we highlight the physical mechanisms and enhancement strategies for synergistic and non-synergistic multicaloric effects under multi-field coupling. This work aims to provide theoretical guidance and technical support for the design and practical implementation of high-performance elastocaloric materials.

2. Elastocaloric effects

The most distinctive advantages of Ni–Mn-based shape memory alloys for elastocaloric applications lie in their low

[†]Corresponding author. E-mail: liujian@shu.edu.cn

© 2026 Chinese Physical Society and IOP Publishing Ltd. All rights, including for text and data mining, AI training, and similar technologies, are reserved.

critical stress for triggering phase transformations and their small stress hysteresis. These characteristics can be attributed to the following three fundamental factors.[10]

(i) The low lattice resistance to transformation originates from the pronounced softening of the TA_2 phonon mode along the $\langle 110 \rangle$ direction, driven by Fermi-surface nesting under strong electron–phonon coupling. This phonon softening indicates a reduction in lattice shear stiffness prior to the transformation, substantially lowering the energy barrier required for the MT and minimizing resistance to lattice reorganization along the $\{110\}\langle -110 \rangle$ shear system. This intrinsically low transformation resistance directly contributes to the low critical stress required to induce the eCE.

(ii) Microstructural texture strongly influences the compatibility of transformation strain and the fatigue resistance of elastocaloric performance. Coarse-grained structures with strong texture can be obtained in Ni–Mn-based alloys through processes such as directional solidification. When the crystallographic orientations of adjacent grains are highly consistent, MT occurs along a specific $\{110\}\langle -110 \rangle$ variant system, allowing the transformation strain directions in each grain to remain similar and enabling effective grain-boundary coordination. This greatly reduces internal stress concentration, energy dissipation, and microcrack nucleation caused by strain incompatibility, thereby ensuring reversible and complete phase transitions and a stable eCE during cyclic loading.

(iii) Since the equilibrium MT temperature must be lower than the test temperature for elastocaloric operation, this temperature deviation introduces additional resistance to transformation. Consequently, initiating MT within the austenite stability region requires the application of excess stress. Incomplete martensite reverse transformation may occur due to insufficient thermodynamic driving force, leading to irreversible residual strain and degradation of elastocaloric performance. This issue can be overcome to some extent through microstructural optimization of Ni–Mn-based alloys, such as introducing coarse grains and strong textures.

Building upon the exceptional functional properties of Ni–Mn-based alloys, extensive research has focused on developing advanced preparation routes and composition designs (including composition optimization and element doping) to overcome their intrinsic brittleness and optimize their microstructure for improved elastocaloric performance, as described below.

2.1. Novel preparation routes

To harness the fundamental elastocaloric advantages outlined above and to mitigate the intrinsic brittleness of Ni–Mn-based alloys, precise control over microstructure through advanced processing is essential. Conventional casting methods (e.g., arc melting and induction melting) are widely used to prepare Ni–Mn-based alloys, but they face two major challenges.[8,10] First, Mn is prone to evaporation during melting due to its high volatility, leading to deviations from the desired composition. Second, dendritic segregation commonly occurs during non-equilibrium solidification, resulting in compositional inhomogeneity. Such inhomogeneity results in local variations in the martensite start temperature (M_s), manifested as a broadened transformation interval (ΔT_{int})) and increased thermal hysteresis (ΔT_{hyst}), ultimately reducing the reversibility of the eCE. To mitigate segregation and composition deviations, homogenization annealing is an essential post-processing step.[8,11] After optimization, the MT characteristics of the alloy, such as transformation temperature and hysteresis, become more stable. However, traditional melting typically yields randomly oriented polycrystalline structures, and grain boundaries remain major sources of crack initiation and functional fatigue, thus limiting long-term cyclic stability. To overcome these limitations, several advanced preparation methods have been developed, including directional solidification, AM, and solidification under high magnetic fields, which are discussed in the following.

2.1.1. Directional solidification

Directional solidification enables preferential crystal growth along a defined heat-flow direction, yielding ingots with coarse columnar or quasi-single-crystal structures.[12,13] This technique generates strong crystallographic textures, eliminates transverse grain boundaries, and improves microstructure and material properties (Fig. 1).[14,15] In Ni–Mn-based Heusler alloys, both the MT and superelastic strain exhibit strong anisotropy, with the $\langle 001 \rangle$ orientation showing the largest recoverable strain. By aligning most grains along this favorable orientation, directional solidification promotes coordinated MT under applied stress, mitigates intergranular stress concentration, and enhances mechanical performance by suppressing crack initiation.[14] Table 1 summarizes the crystallographic orientation, adiabatic temperature change (ΔT_{ad}),

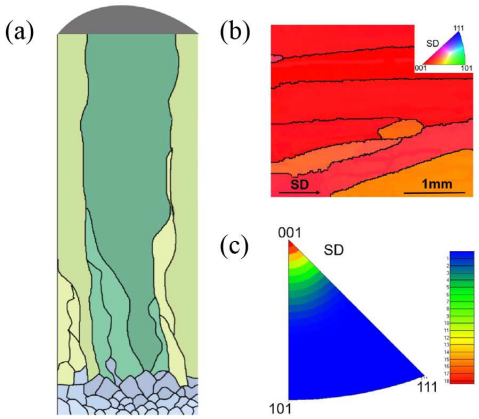


Fig. 1. (a) Microstructure of a directionally solidified sample.[14] (b) Electron backscatter diffraction (EBSD) orientation map taken from the longitudinal section of a directionally solidified $Ni_{55}Mn_{18}Ga_{26}Ti_1$ alloy at RT. (c) Corresponding inverse pole figure along the scanning direction (SD) determined from the EBSD data.[15]

Table 1. Elastocaloric properties of some directionally solidified Ni–Mn-based alloys during unloading.

Alloys	Orientation	ΔT_{ad} (K)	ΔS_{iso} (J·kg^{-1}·K^{-1})	Temperature (K)	Strain rate (s^{-1})	$\Delta\sigma_{max}$ (MPa)	Refs.
$Ni_{50}Mn_{35}In_{15}$	⟨001⟩	19.7	–	320	1.4	350	[16]
$Ni_{50}Mn_{35}In_{13}Si_2$	⟨001⟩	17.7	25.9	RT	1.0	300	[17]
$Ni_{50}Mn_{33}In_{15.5}Cu_{1.5}$	⟨001⟩	11.4	–	290	0.3	150	[18]
$Ni_{55}Mn_{18}Ga_{26}Ti_1$	⟨001⟩	6.2	–	RT	4.0×10^{-2}	120	[15]
$Ni_{50}Mn_{23}Ga_{25}Cu_2$	⟨001⟩	4.3	–	259	4.33×10^{-2}	120	[19]
$Ni_{50}Mn_{30}Ti_{20}$	⟨001⟩	23.7	45.0	293	2.8	1070	[20]
$(Ni_{50}Mn_{31}Ti_{19})_{99}B_1$	⟨001⟩	27.2	38.8	303	3.0×10^{-1}	412	[21]
$Ni_{35.5}Co_{14.5}Mn_{35}Ti_{15}$	⟨001⟩	5.8	–	310	2.1×10^{-2}	180	[22]
$Ni_{44}Mn_{46}Sn_{10}$	⟨001⟩	18.0	–	320	3.0×10^{-1}	390	[23]

isothermal entropy change (ΔS_{iso}), and corresponding test temperature, strain rate, and maximum stress change ($\Delta\sigma_{max}$) for selected directionally solidified Ni–Mn-based alloys during unloading.

In summary, directional solidification significantly enhances the eCE, superelastic behavior, and fatigue resistance of Ni–Mn-based alloys by optimizing the crystallographic texture, reducing the grain-boundary density, and improving the deformation capability, providing an important foundation for their practical application in solid-state refrigeration and actuation.

2.1.2. Additive manufacturing

AM, especially laser powder bed fusion (L-PBF), provides a transformative approach for fabricating Ni–Mn-based elastocaloric alloys. It overcomes fabrication limitations associated with intrinsic brittleness and enables monolithic construction of complex geometries (Fig. 2).[24–27] AM offers two major advantages for elastocaloric material optimization: (i) high geometric freedom enables direct printing of customized heat-exchanger architectures with pores or channels that improve thermal management and device efficiency;[28] (ii) AM suppresses elemental segregation, refines microstructure, and enhances mechanical strength and functional stability.[29] For example, an L-PBF-fabricated $Ni_{45}Mn_{44}Sn_{11}$ alloy subjected to homogenization annealing achieved 99.5% relative density and a compressive strength of 519 MPa, while exhibiting an elastocaloric temperature change of −11 K.[26] In another study, a one-step L-PBF process with high scan speeds (1000–3000 mm·s^{-1}) directly yielded a rapidly solidified austenite phase, resulting in as-built Ni–Mn–Sn alloys with a stable entropy change (ΔS) of 26–31 J·kg^{-1}·K^{-1} and a significant ΔT_{ad} of up to −6.7 K (Fig. 3).[30] These results demonstrate that scanning strategy strongly affects elastocaloric behavior, with loading along the SD enhancing performance due to dominant columnar grain growth and optimized defect distribution.

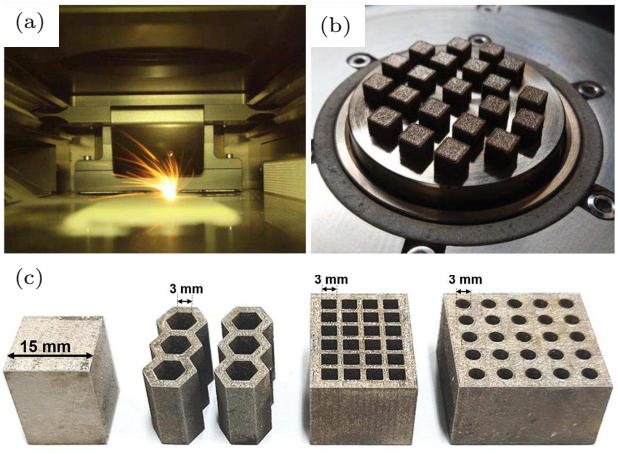


Fig. 2. (a) Processing chamber and (b) as-fabricated samples on a substrate.[27] (c) Complex geometries obtained via AM.[26]

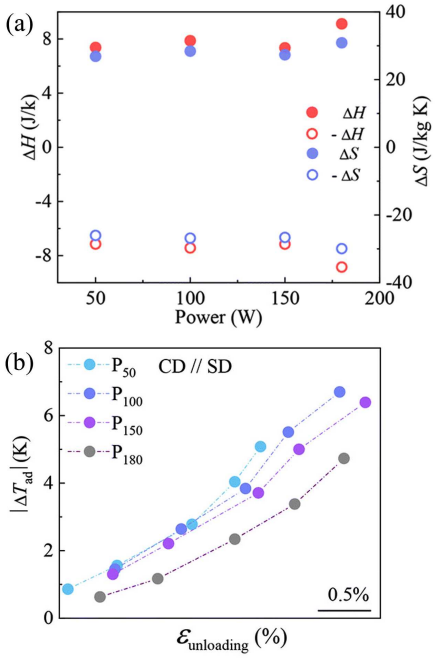


Fig. 3. (a) Enthalpy change (ΔH) and entropy change (ΔS) as a function of laser power. (b) ΔT_{ad} as a function of unloading strain ($\varepsilon_{unloading}$) under compression along the SD of $Ni_{45}Mn_{44}Sn_{11}$ alloys.[30]

However, AM of Ni–Mn-based alloys also faces significant challenges, including a narrow processing window due to high brittleness and crack sensitivity.[31] Repeated laser exposure promotes Mn evaporation and oxidation, altering the composition and affecting phase-transformation behavior.[27] Pronounced residual stresses in as-built components further increase the cracking tendency, particularly in L-PBF.[27,30] Additionally, research on AM-fabricated Ni–Mn-based alloys remains limited, especially regarding direct eCE characterization and cyclic stability.[30]

2.1.3. Solidification under high magnetic field

Solidification under a high magnetic field has emerged as a promising extreme-condition processing technique for material fabrication. Applying a strong static magnetic field introduces non-contact effects, including magnetic alignment and suppression of convection flow, which enable precise control over crystal growth, elemental distribution, and phase selection during solidification.

In directional solidification under such fields, thermoelectromagnetic convection becomes the dominant mechanism, significantly influencing solute transport, phase formation, and crystallographic orientation. The solidification behavior of Ni–Mn–Ga alloys under an axial magnetic field has been systematically investigated.[32] During directional solidification of Ni-rich Ni–Mn–Ga alloys, γ-phase precipitation occurs due to compositional segregation. As illustrated in Fig. 4, moderate magnetic fields (0.5–2 T) generate thermoelectric magnetic convection that radially transports Ni-rich, γ-phase-forming melt from the center toward the periphery. This results in a characteristic ring-shaped distribution, with reduced γ-phase density at the center and increased accumulation at the edges. By contrast, high magnetic fields (≥ 4 T) promote grain refinement, a transition from columnar to equiaxed grains, and microstructural changes including martensite distortion and dislocation reorganization in γ-phase regions. These structural modifications arise from magnetically driven solute redistribution, and numerical simulations show strong agreement with experimental observations.[33]

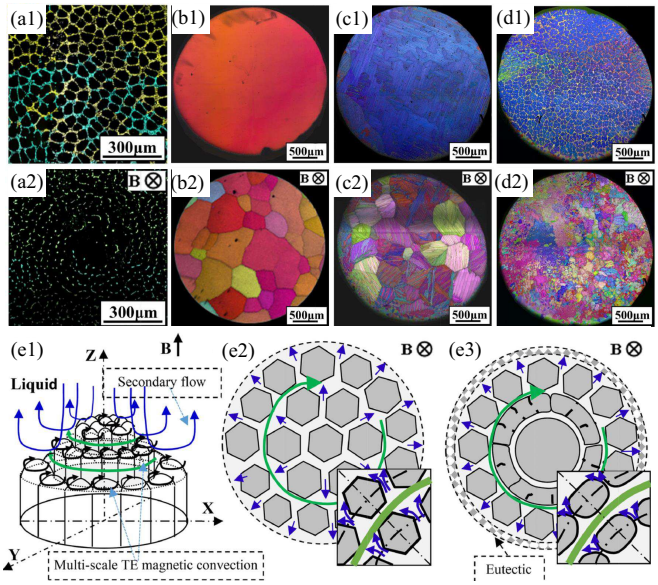


Fig. 4. (a1), (a2) γ phase of $Ni_{58}Mn_{25}Ga_{17}$ alloys under 0 and 2 T. (b1), (b2) Austenite and (c1), (c2) non-modulated (NM) martensite under 0 and 12 T. (d1), (d2) NM martensite and γ phase under 0 and 12 T. (e1)–(e3) Three-dimensional (3D) schematic of thermoelectric (TE) magnetic convection and induced secondary flows across scales.[32]

Under a transverse magnetic field, pronounced transverse macrosegregation has been observed in Ni–Mn–Ga alloys, leading to the formation of martensite clusters embedded within the austenite matrix.[34] Simultaneously, dendrite-arm spacing decreases and microsegregation is reduced, promoting preferential growth along the $\langle 001 \rangle$ orientation. This ability to control crystallographic orientation provides ideal samples for studying crystallography-dependent superelastic behavior. In Ni–Mn–Ti alloys, a transverse magnetic field effectively reduces the critical stress and stress hysteresis, improving the refrigeration capacity and functional stability with a broad working temperature window of 200 K.[35]

These studies not only deepen our understanding of solidification mechanisms under magnetic fields but also establish a new pathway for preparing high-performance elastocaloric materials through multi-field coupling.

2.1.4. Comparative analysis of novel preparation routes for scalability

Directional solidification provides distinct advantages for the large-scale fabrication of shape-memory alloys, enabling the production of sizable ingots with uniform microstructures and a pronounced crystallographic texture along the growth direction. This imparts quasi-single-crystal behavior to polycrystalline materials, thereby enhancing shape-memory responses, mechanical properties, and cyclic stability.[10,22,36,37] However, the technique exhibits notable limitations: the ordered crystal structure of these alloys results in intrinsic brittleness and poor machinability; elemental volatilization during solidification can degrade compositional homogeneity; and the high cost and complex process control associated with producing single-crystal or highly textured materials constrain large-scale commercial viability.[36,37]

AM offers superior design freedom, enabling direct fabrication of intricate porous and lattice structures beyond conventional methods. This supports lightweight design, functional grading, and 4D responsive behavior, making AM well-suited for custom medical devices and small-batch, high-performance parts. However, its large-scale implementation is hindered by high costs, low throughput, and process-induced defects such as pores, micro-cracks, and compositional variation (e.g., Ni evaporation), which degrade functional consistency and fatigue resistance in shape-memory alloys. Surface roughness and residual stress also necessitate extensive post-processing, adding to process complexity and cost.[38]

Solidification under a high magnetic field enables microstructural control from the material source. Magnetically driven thermoelectric convection refines composition distribution, reduces micro-segregation, and promotes strong crystallographic texture, enhancing intrinsic properties such as superelasticity and magnetostriction in alloys and providing high-quality feedstock for further processing.[33,34,39] Its limitations include restriction to simple geometries (e.g., ingots, bars), high equipment costs, and complex process control. Current research remains largely at the laboratory scale, with

scaling to uniform, large-scale production presenting significant engineering challenges.[33,39]

2.2. Composition optimization

Complementary to advances in processing, composition design represents another crucial approach for enhancing the elastocaloric performance of Ni–Mn-based alloys, enabling precise control over phase-transformation characteristics and mechanical properties. Composition design includes tuning the concentrations of principal elements (composition optimization) and introducing additional constituents (element doping).

Composition optimization is a fundamental strategy for tailoring the eCE of Ni–Mn-based alloys. By precisely adjusting the contents of Ni, Mn, and a third element (such as Sn or Ga), key properties, including the MT temperature, transformation hysteresis, entropy change, and microstructure, can be effectively regulated. As illustrated in Fig. 5, the Mn/Sn ratio in Ni–Mn–Sn alloys plays a dominant role in determining the compositional distribution and phase formation, exhibiting substantial variation compared with the relatively stable Ni content.[40] A controlled compositional gradient can broaden the temperature range of magnetic entropy change and increase the refrigeration capacity, although excessive segregation must be avoided to prevent phase instability or the formation of detrimental secondary phases.

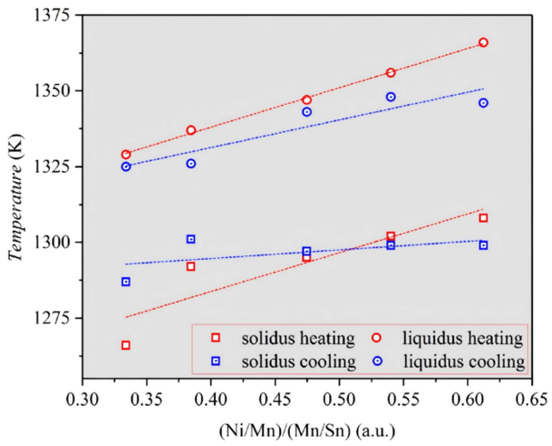


Fig. 5. Solidus and liquidus temperatures of the $Ni_{48}Mn_{39.5}Sn_{12.5}$ determined from onset points during heating and cooling.[40]

In Ni–Mn–Ga systems, a comparative study of 5 M ($Ni_{50}Mn_{28}Ga_{22}$) and 7 M ($Ni_{50}Mn_{30}Ga_{20}$) modulated martensites reveals distinct functional behaviors.[41] The 5 M variant shows a higher ΔS_{iso} (around -1.91 J·kg^{-1}·K^{-1}) but suffers from large thermal hysteresis ($\sim$ 10 K) and low fracture resistance under stresses exceeding the transformation stress. By contrast, the 7 M variant exhibits a lower ΔS_{iso} (around -0.19 J·kg^{-1}·K^{-1}) but features smaller hysteresis ($\sim$ 8 K), higher stress tolerance (up to 18 MPa), and superior reversibility and mechanical stability. These differences are closely related to valence electron concentration per atom (e/a) and modulation type, confirming that composition not only determines transition temperatures but also governs variant microstructure and stress response.

2.3. Element doping

The development of multi-component Ni–Mn-based Heusler alloys addresses key limitations of binary and ternary systems, which, despite their promising eCE and MCE, suffer from narrow transformation intervals, inherent brittleness, large hysteresis, and cyclic degradation. By introducing additional elements via alloying or doping, properties such as phase stability, magnetic exchange interactions, and microstructure can be precisely tailored. This multi-component strategy enables customized material design and advances the practical application of solid-state refrigeration. The following sections describe several element doping strategies, including doping with main-group elements, transition metals, and rare-earth elements.

2.3.1. Doping with main-group elements (Ga, In, Sn, Sb)

In Ni–Mn-based alloys, main-group elements, such as Ga, In, Sn, Ti, and Sb, can be strategically incorporated via partial substitution or micro-doping to precisely tune elastocaloric performance. This approach leverages differences in atomic size and e/a ratio to simultaneously regulate the MT temperature, lattice compatibility, and thermal hysteresis, thereby optimizing the material's eCE response.

As illustrated in Fig. 6, Ga-doped $Ni_{50}Mn_{32}Ti_{16}Ga_2$ exemplifies this strategy: replacing Mn with Ga reduces the e/a ratio, shifts MT temperatures toward RT, and decreases thermal hysteresis from 30 K (undoped) to 21 K, markedly improving reversibility.[42] This alloy achieves a ΔS_{iso} of 23.0 J·kg^{-1}·K^{-1} under only 160 MPa and exhibits a reversible entropy change (ΔS_{rev}) over a wide temperature range of 287–319 K (with a maximum of 20.5 J·kg^{-1}·K^{-1} at 299 K), demonstrating excellent low-stress driving capability. Similarly, in Ni–Mn–In–Ga alloys, Ga incorporation enhances mechanical toughness, enabling stress tolerance above 100 MPa, and strengthens magnetostructural coupling by aligning MT with the Curie temperature, yielding a ΔS_{rev} of 25 J·kg^{-1}·K^{-1} and a ΔT_{ad} of -4.9 K at 100 MPa.[43]

Further enhancement has been observed in a $\langle 001 \rangle$-textured $Ni_{55}Mn_{19}Ga_{25}$ alloy, where substitution of 1 at.% Ti for Ga, combined with directional solidification, raises the compressive strength to 902 MPa and increases the transformation entropy change (ΔS_{tr}) to 29.6 J·kg^{-1}·K^{-1}.[44] This improvement arises from Ti-enhanced coupling between the paramagnetic–ferromagnetic transition and the two-step structural transformation (austenite $\rightarrow$ 7 M $\rightarrow$ NM martensite), resulting in a ΔT_{ad} of -12.9 K under 180 MPa.

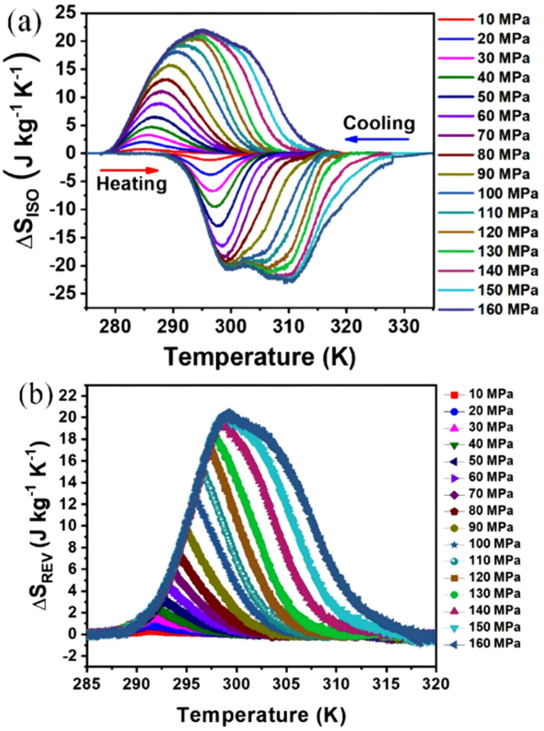


Fig. 6. (a) Isothermal entropy change (ΔS_{iso}) and (b) reversible entropy change (ΔS_{rev}) of $Ni_{50}Mn_{32}Ti_{16}Ga_2$.[42]

However, it should be noted that excessive doping of main-group elements may overshoot the target transformation temperature or introduce undesirable second phases, requiring careful compositional optimization.

2.3.2. Doping with transition metals (Co, Fe, Cu, Cr, etc.)

Transition-metal doping significantly modifies the electronic structure and magnetic properties of Ni–Mn-based alloys, establishing it as a key strategy for enhancing the eCE. Co doping is particularly effective: substituting Co for Ni increases the e/a ratio, strongly suppressing M_s and allowing high-temperature transformation alloys to be tuned toward RT operation. As shown in Fig. 7, a ⟨001⟩-oriented $Ni_{35.5}Co_{14.5}Mn_{35}Ti_{15}$ alloy produced via directional solidification achieves a large ΔT_{ad} of +11.5 K under a low critical stress of 38 MPa, attributed to Co-enhanced magnetoelastic coupling and texture optimization.[22] Co doping also reduces transformation hysteresis, likely through improved parent-phase ordering or lowered interfacial energy. Supporting evidence comes from a hypoeutectic alloy design that disrupts the Kurdjumov–Sachs (K–S) orientation relationship between the $L2_1$ and γ phases, mitigating lattice mismatch and facilitating MT, further confirming the role of Co in regulating transformation behavior.[9] When Co substitutes for Mn, it weakens antiferromagnetic Mn–Mn interactions, stabilizes ferromagnetic order, and fine-tunes transformation characteristics.[45]

Substituting Fe for Mn introduces a smaller magnetic moment than Mn, reducing the overall magnetic moment and typically lowering transformation temperatures. More importantly, Fe doping significantly enhances ductility and toughness while decreasing the critical stress required for stress-induced MT. This improvement is essential for cyclic applications, as it suppresses crack initiation and propagation along grain boundaries, thereby extending functional fatigue life. For example, Fe-doped Ni–Mn–In alloys maintain a stable eCE with $\Delta T_{ad} \approx -4.5$ K over 16000 cycles.[46] Fe-doped Ni–Mn–Al also shows a consistent ΔT_{ad} of −5.1 K over 30 cycles.[47] First-principles studies further reveal that Fe promotes ferromagnetic ordering in austenite and strengthens magnetostructural coupling in Ni–Mn–Ti alloys.[48] Fe-doped Ni–Mn–Ti alloys achieve a record eCE of −24.2 K under only 79 MPa, combined with high strength (2250 MPa) and excellent cyclic stability (> 1800 cycles), as illustrated in Fig. 8.[49]

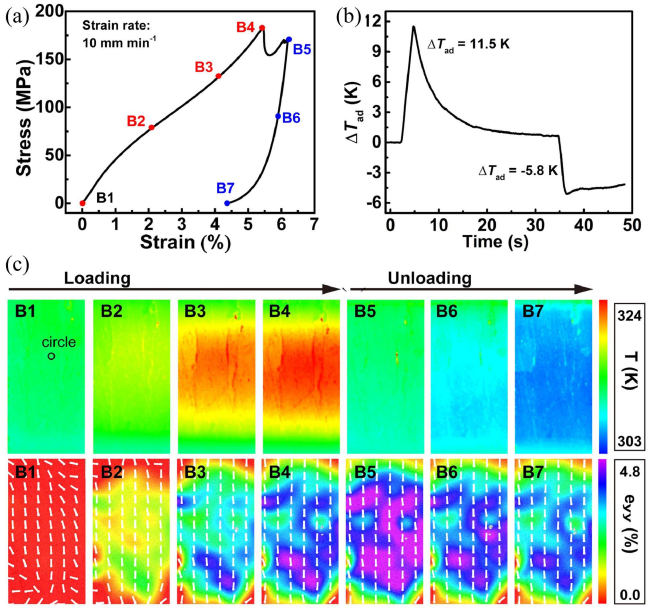


Fig. 7. (a) Stress–strain curve and (b) ΔT_{ad} curve of $Ni_{35.5}Co_{14.5}Mn_{35}Ti_{15}$. (c) Surface temperature and strain fields captured simultaneously by infrared (IR) imaging and digital image correlation (DIC).[22]

Combining Co and Fe yields synergistic enhancements. $Ni_{40}Fe_4Co_6Mn_{32}Al_{18}$ exhibits a ΔT_{ad} of −6.1 K at 400 MPa and retains −5.2 K over 100 cycles, indicating stable cyclic performance.[50]

Cu substitution for Ni markedly reduces transformation hysteresis. Because Cu has a similar atomic size but different chemical characteristics, it promotes local lattice ordering and improves interfacial coherence during transformation. This reduces nucleation barriers, enhances reversibility, and minimizes energy dissipation. In $Ni_{50}Mn_{25-x}Ga_{25}Cu_x$, a Cu content of $x = 6$ produces a thermal hysteresis of only 3 K, directly improving both MCE and eCE efficiency.[51]

Ag enhances mechanical properties through solid-solution and secondary-phase formation. It also raises the e/a ratio, increases the transformation temperature, and aligns

it more closely with the Curie temperature. This alignment reduces negative magnetic entropy contributions, improving the total entropy change and eCE performance. In $Ni_{50}Mn_{34}In_{15.5}Ag_{0.5}$, a ΔT_{ad} of -7 K was achieved at 4% strain, with the fatigue life extended to 69 cycles.[52]

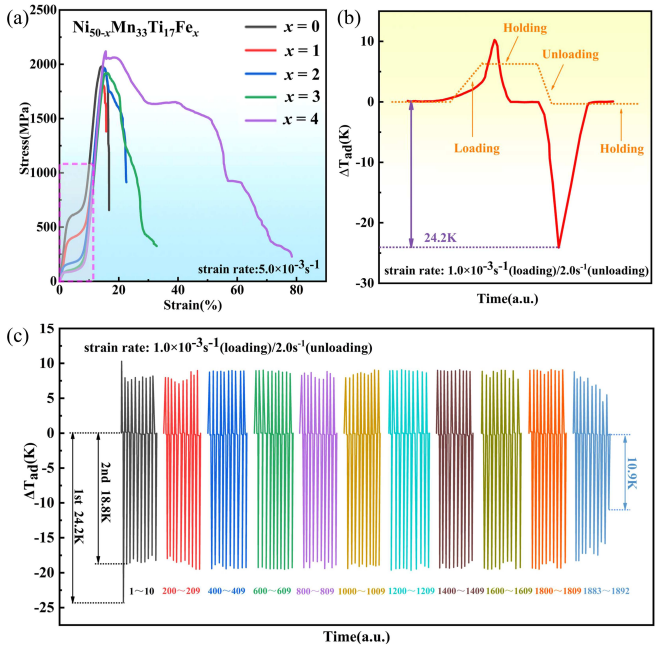


Fig. 8. (a) Stress–strain curves of $Ni_{50-x}Mn_{33}Ti_{17}Fe_x$ ($x = 0$, 1, 2, 3, 4) alloys. (b) ΔT_{ad} curve and (c) cyclic performance of $Ni_{46}Mn_{33}Ti_{17}Fe_4$.[49]

As a high-hardness, non-magnetic element, Zr promotes finely dispersed secondary-phase particles that considerably improve strength and toughness. By increasing the e/a ratio, Zr also elevates the transformation temperature and narrows its separation from the Curie temperature, thereby enhancing both the eCE and MCE. The $Ni_{50}Mn_{34.5}In_{15}Zr_{0.5}$ alloy exhibits a ΔT_{ad} of -8.6 K at 7% strain, demonstrating excellent refrigeration performance.[53]

While transition-metal doping can optimize the properties of Ni–Mn-based alloys, it also introduces notable drawbacks: the strong K–S orientation relationship leads to considerable lattice mismatch strain and suppresses martensitic transformation.[9] Furthermore, doping may promote the formation of hard and brittle secondary phases, which increases material brittleness and raises stress hysteresis, thereby impairing the cyclic stability of the elastocaloric response.[47,49] Hence, doping must be carefully controlled to balance functional performance with mechanical reliability.

2.3.3. Doping with other elements (B, rare earths)

Trace and rare-earth element doping effectively enhances the mechanical and cyclic stability of Ni–Mn-based alloys through microstructural refinement, rather than directly controlling the MT. For instance, adding only 0.3 at.% B to a Ni–Mn–In alloy causes significant grain refinement (from ~ 120 μm to ~ 20 μm) and promotes the formation of a grain-boundary Ni-rich secondary phase, substantially improving intergranular cohesion and fatigue resistance.[54] As shown in Fig. 9, the B-doped alloy $(Ni_{51.5}Mn_{33}In_{15.5})_{99.7}B_{0.3}$ maintains a stable ΔT_{ad} over 7000 cycles without failure, whereas the undoped alloy degrades after only 20 cycles. Although B slightly reduces the transformation temperature and entropy due to secondary-phase formation and an altered e/a ratio, its decisive contribution to cyclic durability makes it essential for practical applications.

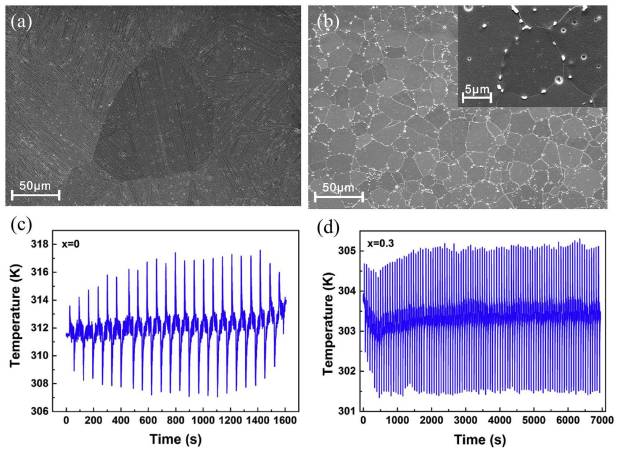


Fig. 9. (a), (b) Scanning electron microscopy (SEM) micrographs and (c), (d) cyclic performance of $(Ni_{51.5}Mn_{33}In_{15.5})_{100-x}B_x$ alloys with (a), (c) $x = 0$ and (b), (d) $x = 0.3$. Inset in (b): magnified view of the microstructure of the alloy with $x = 0.3$.[54]

Rare-earth elements (e.g., Tb, Gd) enhance the performance of Ni–Mn-based alloys through grain-boundary segregation and secondary-phase formation. Their large atomic size and high chemical activity promote the precipitation of rare-earth-rich phases. In Gd-doped (0.6%) Mn–Ni–Sn alloys, γ-phase formation increases the compressive strength from 400 MPa to 1100 MPa while maintaining $\Delta T_{ad} \approx -9.6$ K over 200 cycles.[55] Similarly, Tb doping forms a NiSnTb phase that provides multiple nucleation sites for stress-induced martensite, homogenizes strain, and suppresses crack initiation. This enables $\Delta T_{ad} \approx -5.5$ K to be sustained over 1000 cycles (Fig. 10), demonstrating exceptional functional stability.[56]

Nevertheless, B doping promotes the formation of a secondary phase and alters the matrix composition, which lowers the transformation temperature and entropy change, thereby reducing the intrinsic elastocaloric potential.[54] Rare-earth doping can markedly shift the transformation temperature and increase thermal hysteresis; excessive addition tends to form brittle intermetallic compounds, leading to embrittlement and high sensitivity to the heat-treatment schedule.[56] Therefore, doping must be precisely controlled to balance the enhancement of cyclic stability with the retention of inherent functional performance.

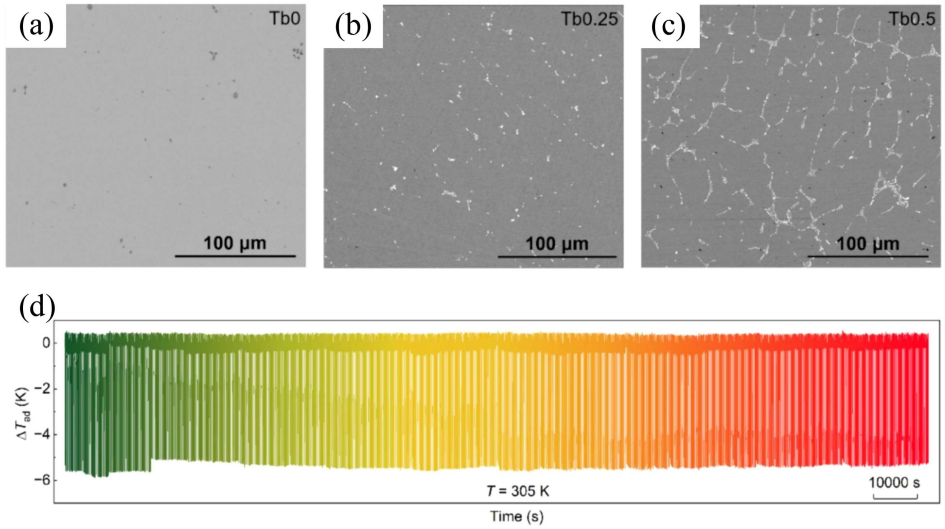


Fig. 10. (a)–(c) SEM images of $(Ni_{43}Mn_{47}Sn_{10})_{100-x}Tb_x$ ($x = 0$, 0.25, 0.5). (d) Cyclic performance of $(Ni_{43}Mn_{47}Sn_{10})_{99.5}Tb_{0.5}$.[56]

The limited cyclic stability of Ni–Mn-based alloys primarily stems from their inherent grain-boundary susceptibility and pronounced transformation-induced strain.[13,34,46] During martensitic transformation, grains with differing orientations undergo incompatible deformation, leading to severe stress concentration at grain boundaries, which readily initiates micro-cracks and promotes premature intergranular fracture. Moreover, the absence of effective microstructural barriers — such as strengthening precipitates — to hinder dislocation motion and crack propagation results in rapid functional degradation under cyclic loading and a generally short fatigue life. Although processing and compositional modifications have enhanced the fatigue resistance of Ni–Mn-based alloys, the achieved cycle numbers remain on the order of 10^2–10^4, representing a core limitation for their engineering applications.[13,15,20,21,34,44,46,47,49,50,52,54–57]

3. Multicaloric effects

Beyond the individual elastocaloric and magnetocaloric effects, the strong magnetoelastic coupling in Ni–Mn-based Heusler alloys gives rise to fascinating multicaloric phenomena under coupled external fields. Owing to their unique magnetostructural coupling, Ni–Mn-based Heusler alloys have become a representative platform for studying the multicaloric effect.

For Ni–Mn-based alloys, MT behavior can be flexibly regulated via synergistic dual-field coupling. This "low-field dual-drive" strategy not only enhances refrigeration performance but also contributes to extending material fatigue life under cyclic loading, offering a promising approach toward efficient, compact, and controllable solid-state refrigeration systems. However, practical implementation faces key challenges, including the inherent trade-off between magnetoelastic coupling strength and giant caloric effects, potential additional stresses induced by magnetic fields on brittle alloys affecting long-term reliability, and the relative complexity and high cost of multi-field actuation systems.[58,59]

According to the interaction between magnetic and structural changes during the phase transformation, these alloys can be classified into two categories: cooperative and non-cooperative. Figure 11 illustrates the schematic of the multicaloric effect and entropy-change coupling in cooperative and non-cooperative systems. In cooperative systems, the magnetic field and stress field act synergistically to promote the MT, resulting in an enhanced caloric effect. In non-cooperative systems, the magnetic field tends to suppress the MT, thereby competing with the stress field. The physical essence of the multicaloric effect lies in the joint modulation of the phase-transition free energy by multiple external fields: the magnetic field influences the magnetic order via the Zeeman energy, while the stress field modifies the lattice stability through elastic energy. The combined application of multiple external fields thus enables precise control over the phase-transition process. The following presents an overview of the achievements made by our research group in the field of the multicaloric effect in recent years.

The Ni–Mn–Ga–In alloy exhibits a pronounced synergistic multicaloric effect (Fig. 12), enabled by its paramagnetic austenite and ferromagnetic martensite, which allow magnetic and stress fields to act cooperatively.[60] Under combined loading conditions (95 MPa and 2 T), ΔT_{ad} reaches −6.7 K, which represents a 72% enhancement compared with the single-field eCE. The underlying mechanism involves a strong coupling between magnetic field and stress, with $dT_{tr}/dH = -0.92$ K/T and $d\sigma_{cr}/dH = -4.1$ MPa/T, indicating that the magnetic field simultaneously promotes transformation and reduces critical stress. This synergy originates from the high Curie temperature of the martensite, where optimized Mn–Mn spacing enhances magnetic exchange interactions. The alloy also shows excellent fatigue resistance over 600 dual-field cycles

and achieves a high refrigeration coefficient of performance (COP) of 14.6, providing a valuable basis for designing cooperative multicaloric materials.

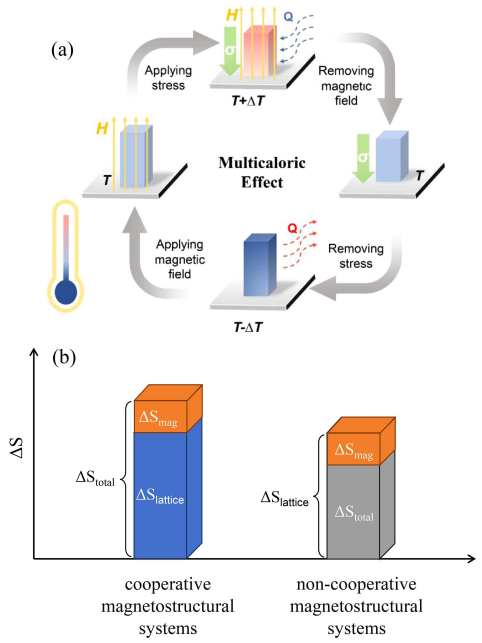


Fig. 11. (a) Schematic of the multicaloric effect driven by multiple fields.[59] (b) Schematic of entropy-change coupling in cooperative vs. non-cooperative phase transitions.

Ni–Mn–Sn alloys fabricated via L-PBF further demonstrate the potential of AM for producing multicaloric materials (Fig. 13).[26] Although rapid solidification suppresses γ-phase formation, it also introduces cracking. Post-process annealing at 1173 K enables effective crack self-healing, yielding a relative density of 99.5% and a uniform equiaxed microstructure with a compressive strength of 519 MPa. The annealed alloy exhibits enhanced transformation entropy and a measurable magnetic entropy change under a field of 5 T. Implementing a magnetic field-assisted elastocaloric refrigeration strategy increases ΔT_{ad} by 20%, reaching -7.4 K. This improvement is attributed to the magnetic stabilization of austenite, which reduces the residual strain from 0.9% to 0.4% and improves the completeness of the reverse transformation, offering a new, promising route for fabricating multicaloric devices.

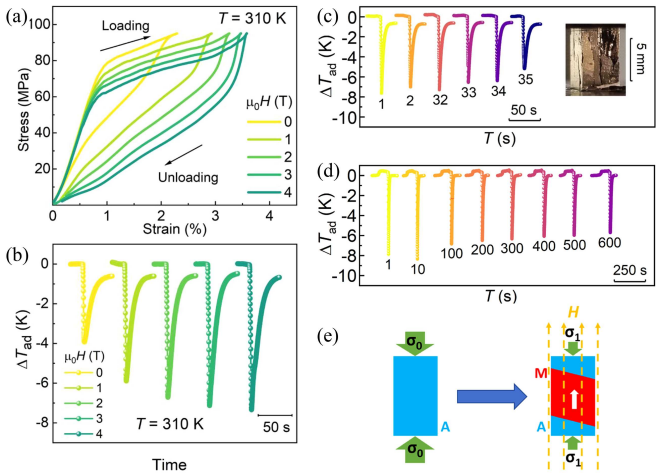


Fig. 12. (a) Stress–strain curves and (b) ΔT_{ad} curves under 0–4 T at 310 K. Cyclic performance under (c) single stress field and (d) dual fields. The inset in (c) shows the sample after 30 cycles under single-field loading. (e) Magnetostress mechanism in Ni–Mn–Ga–In alloys.[60]

Tb-doped Ni–Mn–Sn alloys demonstrate active control over the operating temperature window (Fig. 14).[58] The Tb addition promotes secondary-phase formation, and the associated interfaces act as nucleation sites that lower the energy barrier for transformation. Although the system is non-synergistic ($dT_{tr}/dH = -0.9$ K/T), it still responds effectively to multifield excitation: a 4 T magnetic field increases ΔT_{ad} from -3.5 K to -4.0 K while significantly reducing residual strain. The applied field shifts the operating temperature range by ~ 4 K toward lower temperatures, enabling real-time adjustment of the optimal working temperature. This magnetic-field-induced shift in transition temperature provides an innovative approach for designing adaptive refrigeration systems.

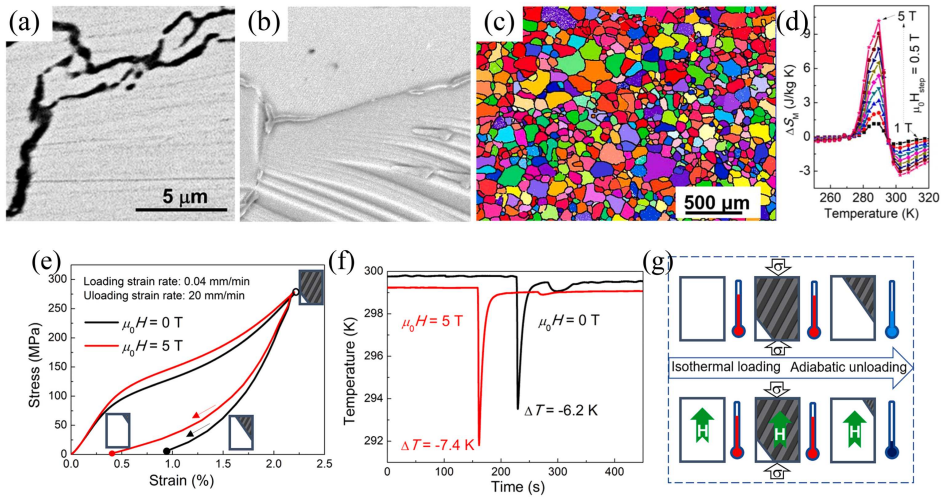


Fig. 13. SEM images (a) before and (b) after the healing treatment. (c) EBSD map after healing. (d) Magnetic entropy change as a function of temperature under different magnetic field changes. (e) Stress–strain curves and (f) ΔT_{ad} curves under 0 and 5 T. (g) Reduced residual martensite under 5 T.[26]

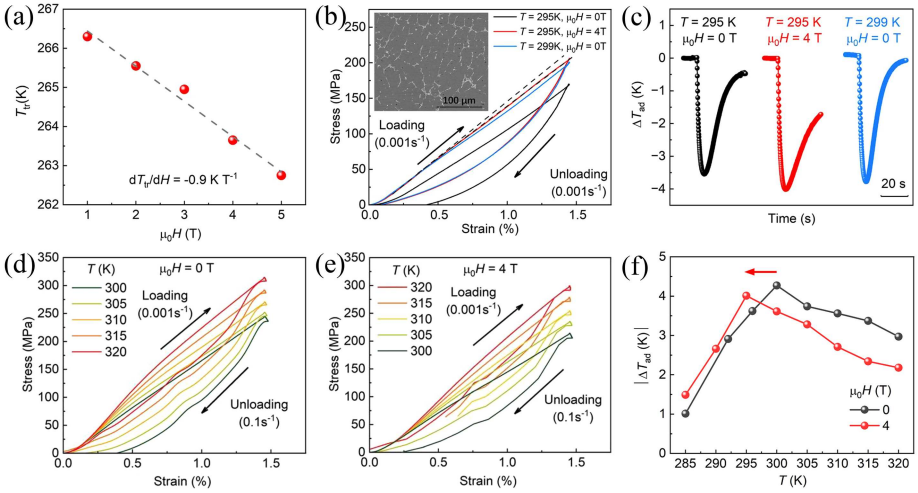


Fig. 14. (a) Magnetic-field sensitivity of the transformation temperature. (b) Stress–strain curves and (c) ΔT_{ad} curves at selected temperatures and fields. The inset in (b) illustrates the SEM image of $(Ni_{43}Mn_{47}Sn_{10})_{99.5}Tb_{0.5}$. Stress–strain curves at different temperatures under (d) 0 T and (e) 4 T. (f) $|\Delta T_{ad}|$ as a function of temperature under 0 and 4 T.[58]

4. Summary and perspectives

Ni–Mn-based Heusler alloys have shown great promise as solid-state refrigerants, with progress driven by coordinated advances in material processing and composition design. This review highlights recent developments in processing techniques, compositional tailoring, and multi-field coupling.

(i) In terms of processing techniques, directional solidification, AM, and solidification under high magnetic fields have enabled textured, low-defect microstructures that improve phase compatibility and suppress cracking. Future research should focus on optimizing laser scanning strategies and exploring solidification under coupled multi-physics fields to achieve finer microstructures and lower residual stress, thereby improving fatigue life.

(ii) Compositional design using main-group and transition-metal elements has effectively tuned transformation temperatures and hysteresis by adjusting e/a ratios and magnetic interactions. The beneficial effects of B and rare-earth micro-alloying on cyclic stability merit further exploration. Future studies should clarify composition–property relationships and explore novel multicomponent systems that combine low driving stress, high entropy change, and mechanical robustness. In addition, future research should focus on establishing quantitative correlations between microstructure and fatigue performance, aiming to extend the cyclic life of Ni–Mn-based alloys to the order of 10^5–10^6 cycles through cross-scale compositional and process design, such as gradient structures and composite architectures.

(iii) Coupling between stress and magnetic fields has been shown to enhance caloric effects synergistically and enable active control over the operating temperature window. A deeper understanding of magnetoelastic mechanisms across different magnetostructural transitions is needed. Future efforts should be devoted to designing optimized multi-field driving cycles based on thermodynamic models and probing material dynamics under coupled fields to fully exploit the potential of multicaloric cooling.

Acknowledgement

This work was supported by the National Natural Science Foundation of China (Grant No. 52371192).

References

[1] Phan M H and Yu S C 2007 *J. Magn. Magn. Mater.* **308** 325
[2] Wang D H, Han Z D, Xuan H C, Ma S C, Chen S Y, Zhang C L and Du Y W 2013 *Chin. Phys. B* **22** 077506
[3] Hou H, Finkel P, Staruch M, Cui J and Takeuchi I 2018 *Nat. Commun.* **9** 4075
[4] Mañosa L, Planes A and Acet M 2013 *J. Mater. Chem. A* **1** 4925
[5] Moya X, Kar-Narayan S and Mathur N D 2014 *Nat. Mater.* **13** 439
[6] Sun W, Liu J, Zhao D and Zhang M 2017 *J. Phys. D: Appl. Phys.* **50** 444001
[7] Ma S, Zhang X, Zheng G, Qian M and Geng L 2023 *Materials* **16** 5725
[8] Villa F, Villa E, Righi L, Ruggieri P, Bennato N, Battiston S, Passaretti F and Casati R 2024 *J. Alloys Compd.* **1000** 175099
[9] Zhai Q, Bu F, Cheng Y, Zhang J and He Y 2025 *J. Magn. Magn. Mater.* **629** 173246
[10] Huang X M, Wang L D, Liu H X, Yan H L, Jia N, Yang B, Li Z B, Zhang Y D, Esling C, Zhao X and Zuo L 2019 *Intermetallics* **113** 106579
[11] Foroozmehr A, Kermanpur A, Ashrafizadeh F and Kabiri Y 2011 *Mater. Sci. Eng. A* **528** 7952
[12] Zheng P, Kucza N J, Wang Z, Müllner P and Dunand D C 2015 *Acta Mater.* **86** 95
[13] Zhang G, Wang Y, Liu C, Cong D, Kuang Y, Yang J, Yang B, Zuo L and Li Z 2025 *Acta Mater.* **301** 121541
[14] Shen Y, Sun W, Wei Z Y, Shen Q, Zhang Y F and Liu J 2019 *Scr. Mater.* **163** 14
[15] Li D, Li Z, Zhang X, Yang B, Wang D, Zhao X and Zuo L 2020 *Scr. Mater.* **189** 78
[16] Li Z, Li Z, Li D, Yang J, Yang B, Hu Y, Wang D, Zhang Y, Esling C, Zhao X and Zuo L 2020 *Acta Mater.* **192** 52
[17] Li Z, Li Z, Lu Y, Lu X and Zuo L 2022 *J. Mater. Sci. Technol.* **117** 167
[18] Wang H, Li D, Zhang G, Li Z, Yang B, Yan H, Cong D, Esling C, Zhao X and Zuo L 2022 *Intermetallics* **140** 107379
[19] Guo J, Wei Z, Shen Y, Zhang Y, Li J, Hou X and Liu J 2020 *Scr. Mater.* **185** 56

[20] Zhang G, Wang H, Li Z, Yang B, Yan H and Zuo L 2023 *Scr. Mater.* **237** 115725

[21] Wang H, Wang Y, Zhang G, Li Z, Yang J, Li J, Yang B, Yan H and Zuo L 2024 *Materials* **17** 4756

[22] Shen Y, Wei Z, Sun W, Zhang Y, Liu E and Liu J 2020 *Acta Mater.* **188** 677

[23] Zhang G, Li Z, Yang J, Yang B, Wang D, Zhang Y, Esling C, Hou L, Li X, Zhao X and Zuo L 2020 *Appl. Phys. Lett.* **116** 023902

[24] Laitinen V, Sozinov A, Saren A, Chmielus M and Ullakko K 2021 *Addit. Manuf.* **39** 101854

[25] Ramezannejad A, East D, Murphy A B, Lu G and Yang K V 2025 *Metals* **15** 488

[26] Sun W, Lu X, Wei Z, Li Q, Li Z, Zhang Y and Liu J 2022 *Addit. Manuf.* **59** 103125

[27] Rittinghaus S K, Shokri H, Shkodich N, Bruder E, Farle M and Gökce B 2023 *Addit. Manuf. Lett.* **7** 100159

[28] Sharma V, Balderson L, Heo R, Bishop O, Hunt C S M, Carpenter E E, Hadimani R L, Zhao H and Barua R 2022 *J. Alloys Compd.* **920** 165891

[29] Laitinen V, Milleret A, Namvari M, De Vecchis P R, Attallah M M, Chmielus M and Ullakko K 2024 *Addit. Manuf.* **90** 104328

[30] Sun W, Qian H, Fu Q, Zhang M, Cheng J, Mo Z, Liu J, Li W and Li G 2024 *J. Mater. Chem. C* **12** 16864

[31] Saren A, Laitinen V, Vinogradova M and Ullakko K 2023 *Acta Mater.* **246** 118666

[32] Hou L, Dai Y, Fautrelle Y, Li Z, Ren Z and Li X 2020 *Acta Mater.* **199** 383

[33] Zhong Q, Zhong H, Han H, Shu M, Hou L, Zhu Y and Li X 2022 *J. Mater. Sci. Technol.* **99** 48

[34] Li X, Hou L, Yang S, Zhou T, Wang Y, Yu X, Li Z, Cong D, Fautrelle Y, Ren Z and Zhu Y 2023 *J. Mater. Sci. Technol.* **142** 10

[35] Wang H, Li Z, Hou L, Li X, Yan H, Yang B and Zuo L 2024 *Acta Mater.* **274** 120020

[36] Wang X, Ding X, Chen R, Ding J, Qian M, Zhang Y and Wu S 2024 *Mater. Sci. Eng. A* **918** 147463

[37] Wang X, Ding X, Chen R, Ding J, Shen H, Qian M, Yang X, Zhang Y and Wu S 2025 *Acta Mater.* **290** 120956

[38] Mehrpouya M, Alberto Biffi C, Lemke J N, Bregoli C, Fiocchi J, Mohajerani S, Tuissi A and Elahinia M 2024 *Virtual Phys. Prototyping* **19** 2414395

[39] Hou L, Dai Y, Fautrelle Y, Li Z, Ren Z, Esling C and Li X 2018 *J. Alloys Compd.* **758** 54

[40] Czaja P, Wierzbicka-Miernik A and Rogal 2018 *J. Cryst. Growth* **492** 50

[41] López-Medina M, Flores-Zúñiga H, Soto-Parra D E and Ríos-Jara D 2024 *Appl. Phys. Lett.* **125** 181905

[42] Ascencio de la Cruz L A, López-Medina M, Soto-Parra D E, Ríos-Jara D, Camarillo-Garcia J P and Flores-Zúñiga H 2024 *Results Phys.* **66** 108009

[43] Camarillo J P, Aguilar-Ortiz C O, Flores-Zúñiga H, Ríos-Jara D, Soto-Parra D E, Stern-Taulats E, Mañosa L and Planes A 2017 *Funct. Mater. Lett.* **10** 1740007

[44] Li D, Zhang X, Zhang G, Li Z, Yang B, Yan H, Wang D, Zhao X and Zuo L 2021 *Appl. Phys. Lett.* **118** 213903

[45] Liang X, Zhang C, Bai J, Gu J, Zhang Y, Esling C, Zhao X and Zuo L 2024 *J. Mater. Sci. Technol.* **172** 156

[46] Pfeuffer L, Lemke J, Shayanfar N, Riegg S, Koch D, Taubel A, Scheibel F, Kani N A, Adabifiroozjaei E, Molina-Luna L, Skokov K P and Gutfleisch O 2021 *Acta Mater.* **221** 117390

[47] Cao T, Xuan H, Liu S, Wang L, Xie Z, Liang X, Chen F, Han P, Wang D and Du Y 2019 *Intermetallics* **112** 106529

[48] Xu J, Bai J, Zhang Y, Guo K, Ma Q, Jiang X, Gu J, Gao Q and Zuo L 2024 *Mater. Today Commun.* **41** 110415

[49] Li B, Li D, Feng Z, Zhu J, Zhong H and Li S 2025 *Mater. Sci. Eng. A* **943** 148778

[50] Xuan H, Wang L, Cao T, Liu S, Xie Z, Liang X, Chen F, Zhang K, Feng L, Han P and Wu Y 2021 *Phys. Lett. A* **402** 127362

[51] Seguí C, Torrens-Serra J, Cesari E and Lázpita P 2020 *Materials* **13** 419

[52] Feng Y, Yuan X, Zhou M and Gao L 2023 *J. Alloys Compd.* **944** 169143

[53] Xie Q, Feng Y, Yuan X, Liu Q, Zhou J and Wang S 2025 *J. Alloys Compd.* **1010** 177765

[54] Yang Z, Cong D Y, Sun X M, Nie Z H and Wang Y D 2017 *Acta Mater.* **127** 33

[55] Wang L, Xuan H, Liu S, Cao T, Xie Z, Liang X, Chen F, Zhang K, Feng L, Han P and Wu Y 2020 *J. Alloys Compd.* **846** 156313

[56] Qian H, Cai R, Lu X, Sun W, Li G, Wei Z and Liu J 2024 *Mater. Des.* **244** 113162

[57] Tang X, Feng Y, Wang H and Wang P 2019 *Appl. Phys. Lett.* **114** 033901

[58] Qian H, Wei Z, Li G and Liu J 2023 *APL Mater.* **11** 111125

[59] Zhang X, Qian H, Cai R, Wei Z, He J, Zhang M, Sun W, Liu J, Felser C and Li G 2024 *ACS Appl. Electron. Mater.* **6** 4440

[60] Qian H, Guo J, Wei Z and Liu J 2022 *Phys. Rev. Mater.* **6** 054401